Molecular Dynamics Simulations of Polymer Networks Undergoing Sequential Cross-Linking and Scission Reactions

Dana R. Rottach,[†] John G. Curro,*[,†] Joanne Budzien,[‡] Gary S. Grest,[‡] Carsten Svaneborg,[§] and Ralf Everaers[⊥]

Department of Chemical & Nuclear Engineering, University of New Mexico, Albuquerque, New Mexico 87131; Sandia National Laboratories, Albuquerque, New Mexico 87185; Department of Chemistry, University of Aarhus, Langelandsgade 140, DK-8000 Århus, Denmark; and Laboratoire de Physique, ENS Lyon, 46, allee d'Italie, 69364 Lyon, cedex 07, France

Received September 14, 2006; Revised Manuscript Received October 29, 2006

ABSTRACT: The effects of sequential cross-linking and scission of polymer networks formed in two states of strain are investigated using molecular dynamics simulations. Two-stage networks are studied in which a network formed in the unstrained state (stage 1) undergoes additional cross-linking in a uniaxially strained state (stage 2). The equilibrium stress is measured before and after removing some or all of the original (stage 1) cross-links. The results are interpreted in terms of a generalized independent network hypothesis. In networks where the first-stage cross-links are subsequently removed, a fraction (quantified by the stress transfer function Φ) of the second-stage cross-links contribute to the effective first-stage cross-link density. The stress transfer functions extracted from the MD simulations of the reacting networks are found to be in very good agreement with the predictions of Flory and Fricker. It was found that the fractional stress reduction upon removal of the first-stage cross-links could be accurately calculated from the slip tube model of Rubinstein and Panyukov modified to use the theoretical transfer functions of Fricker.

1. Introduction

The long-term aging of elastomeric materials is fundamentally different from viscoelastic stress relaxation. Short-term stress relaxation is a function of chain diffusion and reequilibration of a perturbed network. Chemical aging, however, involves changes in the connectivity of the network caused by bond formation and scission.[1−3] Chemical aging shows effects on much longer time scales than the diffusive physical relaxation, determining the changes in elastic properties of polymer networks over years and decades.[4−6] Chemical scission without additional cross-linking is treated by noting that since the cross-linking constraints simply locked in equilibrium network constraints, removing a portion of those constraints produces a network similar to one where the removed cross-links never existed. Hence, the stress depends only on the current value of the cross-link density.[4,5] The effect of scission is to lower the modulus of the network, without affecting its state of ease.

The constitutive behavior of networks is much more complex if the system undergoes cross-linking under strained conditions. In this case the constitutive behavior of the elastomer depends on coupling between the cross-linking and strain histories of the network. Early work, originating with Tobolsky and co-workers,[1−3] established the effect of additional cross-linking (postcuring) on the network properties for the classical affine and phantom models of rubber elasticity. Tobolsky proposed a method for considering the effect of additional cross-link formation in strained networks. For uniaxial tension with a deformation ratio λ, he proposed the *independent network hypothesis* where additional cross-links introduced at $\lambda = \lambda_2$ could be treated as if they formed a separate independent network in parallel to the existing network.

$$\sigma_{\text{total}}(\nu_1,\nu_2,\lambda,\lambda_2) = \sigma(\nu_1,\lambda) + \sigma(\nu_2,\lambda/\lambda_2) \qquad (1)$$

In eq 1, ν_1 is the number density of network chains introduced in the unstrained state $\lambda = 1$ (stage 1) and ν_2 is the number density of network chains introduced at $\lambda = \lambda_2$ (stage 2). The state of ease of the stage 2 network is the state in which the ν_2 additional chains/volume were added. Equation 1 can be used to predict properties of the material, such as the permanent set and stress/strain behavior, provided one has a rubber elasticity theory expression for $\sigma(\nu,\lambda)$. Flory[7] rigorously proved the validity of the independent network hypothesis of Tobolsky for a network of Gaussian chains with the affine deformation assumption. Fricker[8] provided an analogous proof for the phantom Gaussian model, where junctions are allowed to fluctuate and chains are noninteracting. The independent network hypothesis has been used with general constitutive elasticity models by Wineman and co-workers,[9] and various experiments[10,11] on elastomeric networks have tested its efficacy.

Recently,[12,13] we have investigated the independent network hypothesis using molecular dynamics simulations of bead−spring polymer networks formed by cross-linking at two distinct strain states: the initial state of the unstrained network and a subsequent uniaxially deformed state. In our first paper[12] we demonstrated that the stress recorded in the strained state ($\lambda = \lambda_2$) was not affected by additional cross-link formation in accordance with eq 1, providing direct evidence of the accuracy and utility of the independent network hypothesis. These additional cross-links, however, were observed in the elastic properties of the network when the applied stress was removed. The networks exhibited a significant permanent set. In our second paper[13] we used MD simulations to determine the permanent set of networks postcured in the strained state. These MD results were compared with predictions from the indepen-

[†] University of New Mexico.
[‡] Sandia National Laboratories.
[§] University of Aarhus.
[⊥] ENS Lyon.

10.1021/ma062139l CCC: $37.00
Published on Web 01/02/2007

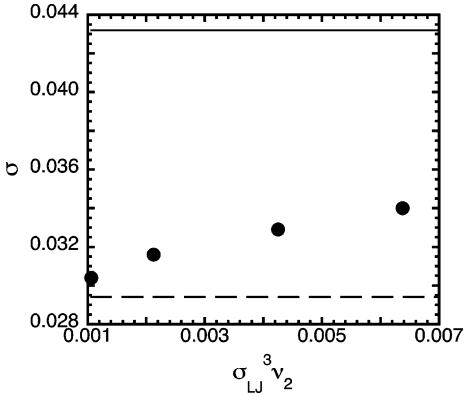

Figure 1. Stress at $\lambda_2 = 2.0$ for a two-stage network with all the first stage cross-links removed (points). The upper solid line represents the stress before any cross-links are removed. The dashed line is the entanglement contribution to the stress.

dent network hypothesis used together with various rubber elasticity theories. Models that include entanglement constraints, specifically the slip tube model of Rubinstein and Panyukov[14] and the double tube model of Everaers,[15,16] were in very good agreement with the simulations.

In actual applications of elastomeric materials, it is usually the case that both scission of old cross-links and formation of new cross-links occur simultaneously.[1] The purpose of this paper is to study the simpler case of sequential cross-linking and scission occurring in a strained network. Flory and Fricker predicted a reinforcement of the earlier network through a partial transfer of effective network chains with *stress transfer functions* for the affine and phantom models, respectively.[7,8] In this work we started with two-stage networks formed by introducing ν_1 network chains per volume in the unstrained state, followed by the introduction of a ν_2 network chain density in the uniaxial strain state at $\lambda = \lambda_2$. We then used MD simulation to determine the stress at $\lambda = \lambda_2$ when some or all the original cross-links formed in the unstrained state were removed. We will first discuss a generalization of the independent network hypothesis to describe simultaneous scission and cross-linking. We will then review the computer simulation methods used to study reacting networks. Results will be presented for the *stress transfer function* needed to obtain effective stage 1 and stage 2 cross-link densities. Finally, the generalized independent network hypothesis will be used with the slip-tube model to compute the stresses of stage 2 networks undergoing cross-linking and scission. Comparisons will be made between the theoretical predictions and our MD simulations.

2. Generalized Independent Network Hypothesis

Consider what happens to the stress of a two-stage network when all of the original stage 1 cross-links added after network formation are subsequently removed so that $\nu_1 = 0$. According to the independent network hypothesis in eq 1, if the deformation ratio is held at $\lambda = \lambda_2$, the stress would decrease to σ_e, the stress due only to trapped entanglements when the network was cross-linked in the melt state. A rather surprising result was found as illustrated in Figure 1. The upper line in this figure is the stress prior to the removal of all the original (first-stage) cross-links. The dashed line in Figure 1 corresponds to the entanglement stress. The stress from the MD simulation, however, is significantly greater than the entanglement contribution in violation of the independent network hypothesis. A naïve application of the independent network model developed in our previous paper[13] would suggest that the stress for such a network

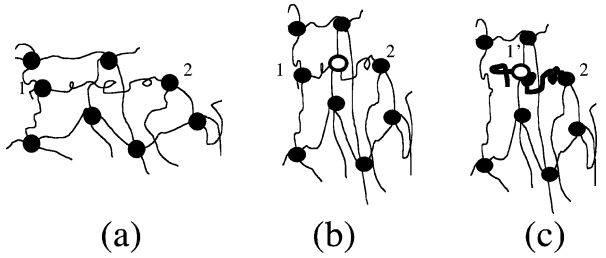

Figure 2. Schematic example of a mechanism for the stress transfer of stage 2 to stage 1 cross-links. (a) A network is formed in the unstrained state at stage 1 with the cross-links denoted as solid circles. (b) The network is strained and a stage 2 cross-link is introduced denoted by the open circle. (c) One of the stage 1 cross-links is removed, and the stage 2 cross-link now assumes the role of the removed stage 1 cross-link.

should simply be the stress due to the entanglements locked into the first stage, represented by the lower (dashed) line. The recorded stress, however, varies monotonically with increasing stage two cross-link density, indicating that cross-links added in the second stage before the removal of the original cross-links retain some memory of those earlier cross-links. The details of the network simulations will be presented in the next section.

The failure of the original independent network hypothesis for networks undergoing scission was addressed for Gaussian networks by Flory[7] for the affine model and by Fricker[8] for the phantom network model. In Figure 2 we can see intuitively why the independent network hypothesis breaks down. Panel (a) depicts a stage 1 network where the cross-links (filled circles) were introduced at zero strain. In particular, let us focus on the network chain 1−2 between cross-links labeled 1 and 2. In panel (b) a two-stage network is created by uniaxially deforming to λ_2 the stage 1 network and introducing a stage 2 cross-link (open circle). No additional stress arises because this stage 2 cross-link is at its state of ease at λ_2. Hence, the network chain 1−2 is unchanged by the presence of the new stage 2 cross-link. In panel (c) we removed the original stage 1 cross-link labeled 1. Note that now the stage 2 cross-link (now labeled 1′) takes over the role of the removed cross-link by preserving the original network chain 1−2 that would be otherwise elastically ineffective. Thus, the stage 2 cross-links play the role of the stage 1 cross-links that are removed from the network due to scission.

By considering the intrachain distribution function in an affinely deformed network, Flory[7] derived a distribution of segment extensions in a network formed in two stages. When no cross-links are removed, the independent network model is shown to be rigorous. By considering the distributions after some of the first stage cross-links are removed, Flory deduced a stress transfer function Φ that represents the fraction of stage 2 cross-links that assume the role of the removed stage 1 cross-links. The independent network hypothesis in eq 1 can thus be preserved by replacing ν_1 and ν_2 in eq 1 by the *effective* densities of network chains ν_1^{eff} and ν_2^{eff}.

$$\sigma_{\text{total}}(\nu_1^{\text{eff}},\nu_2^{\text{eff}},\lambda,\lambda_2) = \sigma(\nu_1^{\text{eff}},\lambda) + \sigma(\nu_2^{\text{eff}},\lambda/\lambda_2) \qquad (2)$$

The total number of effective cross-links is equal to the total number of cross-links remaining in the system, with Φ apportioning second-stage cross-links between stages.

$$\nu_1^{\text{eff}} = \nu_1 + \Phi\nu_2$$
$$\nu_2^{\text{eff}} = (1 - \Phi)\nu_2 \qquad (3)$$

Flory[7] obtained the following expression for the stress transfer function of an affine network

$$\Phi = 2pqs\sum_{\kappa=1}^{\infty}[(1-q-s)/(1-p)(1-q)]^{\kappa-1} \times \sum_{\varsigma=1}^{\infty}[\varsigma/(\varsigma+\kappa)](1-p)^{\varsigma+\kappa}\sum_{\eta=1}^{\infty}[\eta/(\eta+\kappa)](1-p)^{\eta+\kappa} \Big/ (1-p)^2(1-q)^2 \quad (4)$$

where $p = \nu_1^*/\rho_m$, $q = (\nu_1 + \nu_2)/\rho_m$, and $s = (\nu_1^* - \nu_1)/\rho_m$. ν_1^* and ν_1 represent the number density of stage 1 network chains before and after removal, respectively, and ρ_m is the monomer density. For the case when all the stage 1 cross-links are removed (i.e., $\nu_1 = 0$), eq 4 can be approximately written in closed form as[7]

$$\Phi \cong \frac{2}{3}\left[\frac{\nu_T}{\nu_2} + \frac{\nu_2}{\nu_1^*}\ln\left(\frac{\nu_2}{\nu_T}\right) + \left(\frac{\nu_1^*}{\nu_2}\right)^2 \ln\left(\frac{\nu_1^*}{\nu_T}\right)\right] \quad (5)$$

for the affine model where $\nu_T = \nu_1^* + \nu_2$.

For the case of the phantom network model, Fricker[8] deduced an approximate expression for the stress transfer function that is much simpler than the corresponding Flory expression in eq 4.

$$\Phi \cong \frac{\nu_1^* - \nu_1}{\nu_T} \quad (6)$$

Note that Fricker's approximation remains valid for phantom networks when any portion of the initial cross-link density is removed. These theoretical forms of the stress transfer functions will be tested by comparing with stress transfer functions obtained directly from our MD simulations.

3. MD Simulations

In this investigation we performed MD simulations to study the effects of scission of stage 1 cross-links in two-stage networks. Two-stage networks were prepared[12,13] in a sequence where (i) a melt of linear chains is cross-linked at zero strain (stage 1), (ii) the system is elongated at constant volume to a stretch ratio of λ_2 where additional cross-links are introduced (stage 2), and (iii) a portion (or all) of the stage 1 cross-links formed above the concentration required for network percolation are removed. This sequence is illustrated schematically in the first two panels in Figure 2. Stage 1 networks originated from an equilibrated melt of linear chains where sufficient cross-links are introduced to be well above the gel point. A uniaxial strain (at constant volume) was then applied followed by the introduction of additional cross-links to form the second-stage. To match Flory's notation,[7] we use ν_1^* and ν_2 to denote the number density of network chains (twice the cross-link density for tetrafunctional junctions) introduced at stages 1 and 2, respectively, and ν_1 the number density of stage 1 network chains remaining.

As in our previous studies, we employed the standard bead−spring model[17,18] for the polymers where the beads interact through a truncated Lennard-Jones potential

$$V(r) = 4\epsilon\left[\left(\frac{\sigma_{LJ}}{r}\right)^{12} - \left(\frac{\sigma_{LJ}}{r}\right)^{6} + \frac{1}{4}\right] \qquad r \le 2^{1/6}\sigma_{LJ}$$
$$= 0 \qquad r > 2^{1/6}\sigma_{LJ} \quad (7)$$

where σ_{LJ} and ϵ are the Lennard-Jones parameters. A FENE potential interaction[16] is added between bonded sites, either on the original chain or between cross-linked sites

$$V_{FENE}(r) = -\frac{k}{2}R_0^2\ln[1-(r/R_0)^2] \qquad r \le R_0$$
$$= \infty \qquad r > R_0 \quad (8)$$

where $R_0 = 1.5\sigma_{LJ}$ and $k = 30\epsilon/\sigma_{LJ}^2$. MD simulations were performed in a NVT ensemble using the LAMMPS parallel MD code.[19] The simulations typically used between 18 and 36 processors, with individual runs using ~1700 processor hours/million time steps. The molecular dynamics time step was 0.01τ where the characteristic time is $\tau = \sigma_{LJ}(m/\epsilon)^{1/2}$ in Lennard-Jones units, and m is the mass of a bead. The simulations employed periodic boundary conditions at a reduced monomer density $\rho\sigma_{LJ}^3 = 0.85$ and reduced temperature $k_BT/\epsilon = 1$. MD simulations were used to prepare two sets of networks,[13] denoted as A and B, that differ in the way cross-links are introduced and removed.

Network A started from a melt having 500 chains of 500 sites each. Four percent of the sites on each chain were randomly designated as reactive, subject to the condition that pairs of reactive sites were separated by at least two bonds. The system was equilibrated before any reactions were performed. At regular time intervals the MD simulation was stopped, and the distances between all pairs of reactive sites were evaluated. Pairs of sites within a capture radius of $1.3\sigma_{LJ}$ were then covalently bonded with some probability q. The time intervals between reactions and q were adjusted so that quasi-equilibrium conditions were maintained. The cross-linking reactions exhibited second-order kinetics[12] until high conversions where the reaction becomes diffusion-controlled. Networks A were determined to have a gel point at $\nu_{gel} = 0.00326/\sigma_{LJ}^3$. Network A samples were cross-linked to various levels ($\nu_1 = 0.0068/\sigma_{LJ}^3$, $0.0136/\sigma_{LJ}^3$, and $0.0204/\sigma_{LJ}^3$), corresponding to average degrees of polymerization between chemical cross-links of 125, 62.5, and 41.7 sites, respectively.

Network B originated from a melt of 80 chains of 3500 monomers. By contrast with network A, the cross-links in network B were introduced in a single step. The melt of chains was equilibrated in the unstrained state, after which 1400 or 2800 randomly chosen pairs of sites within a capture radius $1.3\sigma_{LJ}$ were cross-linked instantaneously. This corresponds to an average degree of polymerization between cross-links of 100 monomers ($\nu_1 = 0.0085/\sigma_{LJ}^3$) or 50 monomers ($\nu_1 = 0.017/\sigma_{LJ}^3$), respectively. Because the initial chains are much longer in network B than A, the gel point occurs at lower cross-link densities estimated[20,21] as $\nu_{gel} = 0.00029/\sigma_{LJ}^3$).

Both networks A and B started with a cubic, periodic box with sides L_0 in the unstrained state. The networks were uniaxially deformed by changing the box length to λL_0 in the x direction and to $L_0/\sqrt{\lambda}$ in the y and z directions so the volume remains constant. This deformation is accomplished by a series of small affine deformations, $\{x_i,y_i,z_i\} \rightarrow \{x_i\Delta\lambda, y_i/(\Delta\lambda)^{1/2}, z_i/(\Delta\lambda)^{1/2}\}$ until the desired strain is achieved. The molecular dynamics simulation proceeded during the constant-volume deformation process, so that even though the individual small steps were affine, the network was allowed to adjust, so that the overall deformation was nonaffine. The stress σ_x in the direction of strain is obtained from the simulation through the stress tensor P_{ij} according to[15]

$$\sigma_x = \frac{3}{2}P_{xx} - \frac{1}{2}\sum_i P_{ii} \tag{9}$$

The networks were deformed to an extension ratio of λ_2, and stage 2 cross-links were added to the system. For the network A simulations, the system was equilibrated for $\sim 2 \times 10^4\tau$, after which the stage 2 cross-links were added gradually at the same rate as in stage 1. For network B the stage 2 cross-links were added immediately after deformation. After the second stage cross-links were introduced, both networks A and B were equilibrated for $(1-2) \times 10^5\tau$; the stress was averaged over the last $(3-5) \times 10^4\tau$ which is sufficient to achieve equilibration.[13] After obtaining the stresses for the various two-stage networks, various numbers of the original stage 1 cross-links were removed. The networks were then reequilibrated, and the stresses were again determined. In both the A and B networks, the stage 1 cross-links were removed in one step. Tables 1 and 2 summarize the various networks that were studied.

4. Results

As described above, we prepared various networks in which old (stage 1) cross-links are removed and new (stage 2) cross-links are introduced while the system is strained. Does this complicated cross-linking process affect the connectivity of the resulting networks? To address this question, we analyzed the distribution of network chains of the networks with different cross-linking histories. These results are shown in Figure 3 for the B networks. It can be seen that all the distributions agree with an exponential distribution function expected for systems where four-functional cross-links are introduced in a random, uncorrelated way. Thus, the network chain distributions of the various networks appear to be independent of the cross-linking history and strain.

The stresses were obtained before and after removal of the stage 1 cross-links from MD simulations for both the A and B networks. These results are displayed in Tables 1 and 2. It is possible to use this data to infer the stress transfer functions of the various systems in a model-free manner, without invoking any particular rubber elasticity theory. This can be achieved by estimating the network chain density of a single-stage network that has the same stress as the two-stage network with some of the stage 1 cross-links removed. By definition, this network chain density corresponds to ν_1^{eff}. Equation 3 can then be used to obtain the stress transfer function

$$\Phi = \frac{\nu_1^{\text{eff}} - \nu_1}{\nu_2} \tag{10}$$

from ν_1 and ν_2 of the two-stage network of interest. To make this estimate, we performed MD simulations on single-stage A and B networks, at a fixed elongation $\lambda = 2.0$, at three different cross-link densities. These results are shown in Figure 4 for both networks A and B. The networks, while similar, do not exhibit exactly the same stress/strain relationship. As seen in this figure, a linear dependence of the stress on ν is found for both networks.

Figure 4 was then used to estimate ν_1^{eff} by interpolation for all the two-stage networks studied with the results tabulated in Tables 1 and 2. We can now compare these stress transfer functions from our MD simulations with the corresponding predictions from the Flory[7] theory for affine networks and the Fricker[8] theory for phantom networks given by eqs 5 and 6, respectively. This comparison between simulation and theory is given in Figure 5a for the A networks and Figure 5b for the B networks. Remarkably, both Flory's and Fricker's predictions are in reasonable agreement with the simulation values of Φ within the errors of the simulation. Note that the theoretical predictions for the stress transfer function were accurate despite the fact that the affine and phantom models are known to be quantitatively inaccurate. In fact, our previous MD investigations[13] on identical networks indicated that inclusion of entanglement effects is essential for the accurate prediction of the permanent set. It can be seen from Figures 5 that the phantom model seems to provide a somewhat more accurate prediction for Φ than the affine model. This is consistent with our earlier findings[13] where the phantom model was found to be more accurate ($\alpha = 0.39$) than the affine model for predicting the stresses at small strains.

Table 1. Stress Transfer Function Results from Networks A[a]

$\sigma_{LJ}^3(\nu_1^* - \nu_{gel}) \times 10^3$	$\sigma_{LJ}^3\nu_2 \times 10^3$	$\sigma_{LJ}^3(\nu_1 - \nu_{gel}) \times 10^3$	Φ	$[\sigma] \times 10^3(\epsilon/\sigma_{LJ}^3)$
3.5	6.8	0	0.32	8.71
3.5	13.6	0	0.13	8.49
3.5	20.4	0	0.13	9.00
10.3	6.8	0	0.64	9.34
10.3	6.8	3.5	0.43	10.5
10.3	13.6	0	0.32	9.34
10.3	13.6	3.5	0.23	10.6
17.1	6.8	0	0.86	9.86
17.1	6.8	3.5	0.60	10.8
17.1	6.8	10.3	0.26	13.1

[a] 500 chains of 500 monomers. Initially 1000, 2000, or 3000 cross-links were added and the resultant network strained to $\lambda_2 = 2.0$. Reactions continued until 1000, 2000, or 3000 additional cross-links (to a maximum total number of cross-links of 4000) were added. First stage cross-links above the gel point were removed before the stress was recorded.

Table 2. Stress Transfer Function Results from Networks B[a]

$\sigma_{LJ}^3(\nu_1^* - \nu_{gel}) \times 10^3$	$\sigma_{LJ}^3\nu_2 \times 10^3$	$\sigma_{LJ}^3(\nu_1 - \nu_{gel}) \times 10^3$	Φ	$[\sigma] \times 10^3\,(\epsilon/\sigma_{LJ}^3)$
4.11	1.06	0	0.56	8.69
4.11	2.13	0	0.61	9.03
4.11	4.25	0	0.49	9.40
4.11	6.38	0	0.43	9.71
8.21	4.25	0	0.68	9.80
8.21	8.50	0	0.60	10.9

[a] 80 chains of 3500 monomers. Initially 1400 or 2800 cross-links were added and the network strained to $\lambda = 2.0$. 350, 700, 1400, or 2800 more cross-links added and the all of the initial cross-links taken away.

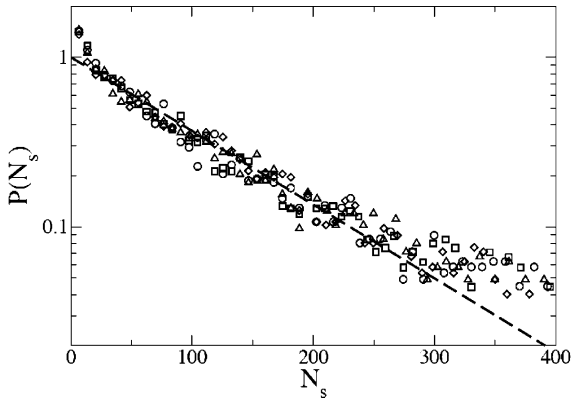

Figure 3. Network chain distribution for B networks with 1400 initial stage 1 cross-links with various cross-linking histories: 1400 stage 1 cross-links (circles); 1400 stage 2 cross-links at $\lambda_2 = 2$ (squares) and $\lambda_2 = 4$ (diamonds) with all stage 1 cross-links removed; 2800 first stage cross-links replaced by 1400 s stage cross-links at $\lambda_2 = 2$ (triangles). The dashed line is an exponential distribution $P(N_s) = \exp[-N_s/\langle N_s\rangle]$ with $\langle N_s\rangle = 100$, which follows from the assumption that the chains are randomly cross-linked.

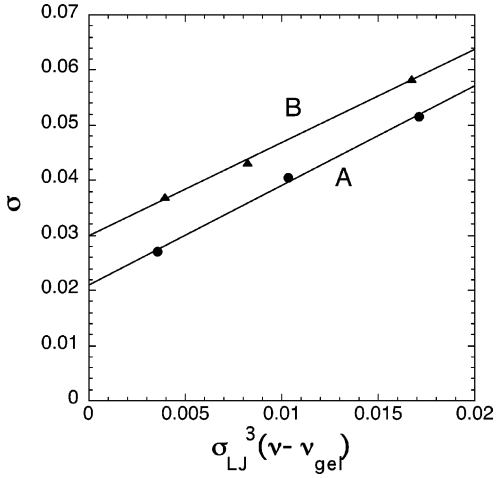

Figure 4. Deviatoric stresses for single stage A and B networks at $\lambda_2 = 2$. Lines show best linear fits. Points are from MD simulations.

5. Discussion

5.1. Constitutive Model. The fact that the Flory and Fricker formulas for the stress transfer function agreed with the simulations suggests that these formulas are not restricted to just the affine or phantom models but may have more general applicability. This leads us to speculate that Φ calculated from eqs 4, 5, or 6 could be applied to other constitutive models as well. Thus, one could use the Flory or Fricker stress transfer functions to obtain the effective network chain densities ν_1^{eff} and ν_2^{eff} in the generalized independent network hypothesis when used with a more accurate rubber elasticity theory that includes entanglement effects. Ideally, one would like to treat the network connectivity and the entanglement effects (which, once locked-in during network formation, are essentially fixed) within an encompassing framework based on network topology. Attempts to treat rubber elasticity with this topological approach have quickly mired in complexity.[22] The most successful recent models have therefore treated connectivity and entanglements as separate effects, which are then combined in some manner.[14−16,23−26] The constrained junction,[23] constrained mode,[15] and the double tube models[16] combine the effects before weighting accessible network conformations. This approach, while conceptually satisfying, greatly complicates calculations. Some tube models[14,24,25] first calculate the stress due to entanglements and then add a separate phantom network stress term to account for the effect of network connectivity. Models of this sort are more mathematically tractable. Here we will test the concept of effective stress transfer using a model of this sort, the slip-tube model of Rubinstein and Panyukov.[14] For this purpose we calculated the ratio of stresses (at $\lambda = \lambda_2$) before and after removal of $\nu_1^* - \nu_1$ stage 1 network chains per unit volume and compared with the simulation results in Tables 1 and 2. The model depends on two parameters: the entanglement modulus and the phantom modulus (itself a function of cross-link density). In our previous paper,[13] parameters were obtained by extrapolating values recorded at finite strain to the $\lambda = 1.0$ limit. We obtain a value of $G_e = 0.0081kT$ and a linear relationship between cross-link density and phantom modulus, $G_{ph} = \alpha\nu kT$, where $\alpha = 0.39$. For completeness, we also made a similar comparison based on the affine/phantom model.

The generalized independent network hypothesis in eq 2, when used with the affine[27] or phantom[28] models, takes the form

$$\sigma(\nu_1^{\text{eff}},\nu_2^{\text{eff}},\lambda,\lambda_2) = \alpha\nu_1^{\text{eff}}k_BT\left(\lambda^2 - \frac{1}{\lambda}\right) + \alpha\nu_2^{\text{eff}}k_BT\left(\frac{\lambda^2}{{\lambda_2}^2} - \frac{\lambda_2}{\lambda}\right) \quad (11)$$

where $\alpha = 1$ (1/2) for the affine (phantom) model. Note that when the network is held fixed at $\lambda = \lambda_2$, the second term in eq 11 drops out. Thus, for both the affine and phantom models, the stress ratio before and after removal of cross-links has the simple form given by

$$\frac{\sigma(\nu_1)}{\sigma(\nu_1^*)} = \frac{\nu_1^{\text{eff}}}{\nu_1^*} = \frac{\nu_1 + \Phi\nu_2}{\nu_1^*} \quad (12)$$

Equation 12 can be seen to be independent of λ_2 and α for the affine and phantom models.

Entanglement effects in polymer networks have recently been treated as harmonic potentials forming effective tubes around the primitive path of the polymer.[14−16,25] In contrast to the junction-based models,[29,30] tube models not only constrain fluctuations at the junctions but also restrict the motions of the intervening polymer segments. The entanglement contribution to stress in tube models complicates the calculation of the network stress transfer. We will examine the slip-tube model developed Rubinstein and Panyukov,[14] which represents the effect of entanglements by mobile rings defining a tube surrounding the Gaussian network backbone. As in our previous work,[13] we will use the tractable approximation of the stress for the slip-tube model provided by Rubinstein and Panyukov

$$\sigma = \sigma_e(\lambda) + \alpha k_BT\nu_1^{\text{eff}}\left(\lambda^2 - \frac{1}{\lambda}\right) + \alpha k_BT\nu_2^{\text{eff}}\left(\frac{\lambda^2}{{\lambda_2}^2} - \frac{\lambda_2}{\lambda}\right) \quad (13)$$

where the entanglement stress is approximated by

$$\sigma_e(\lambda) = \frac{G_e(\lambda^2 - \lambda^{-1})}{0.74\lambda + 0.61\lambda^{-1/2} - 0.35} \quad (14)$$

for the slip-tube model. G_e is the entanglement shear modulus in the limit of small strain.

$$G_e = \nu_e kT \quad (15)$$

which was found[13] previously to be $G_e = 0.0081\epsilon/\sigma_{LJ}^3$ for both our A and B networks. Equation 15 serves as our definition of the chain density ν_e, which corresponds[13] to $\nu_e = 0.0081/\sigma_{LJ}^3$. Because of the entanglement term in eq 13, the stress ratio obtained from the slip-tube model is more complex than from the affine/phantom models.

$$\frac{\sigma(\nu_1)}{\sigma(\nu_1^*)} = \frac{\sigma_e(\lambda_2) + \alpha k_BT(\nu_1 + \Phi\nu_2)\left({\lambda_2}^2 - \frac{1}{\lambda_2}\right)}{\sigma_e(\lambda_2) + \alpha k_BT\nu_1^*\left({\lambda_2}^2 - \frac{1}{\lambda_2}\right)} \quad (16)$$

Note that the stress ratio for the slip-tube model depends explicitly on the factor α. We found previously[13] that a value of $\alpha = 0.39$ is needed to obtain agreement with the MD simulations of our networks in the small strain limit.

In Figure 6a,b we plotted the stress ratio predictions from the affine/phantom and slip-tube models using the Fricker formula in eq 6 for the stress transfer function. Also plotted are the results from MD simulations of the A networks where

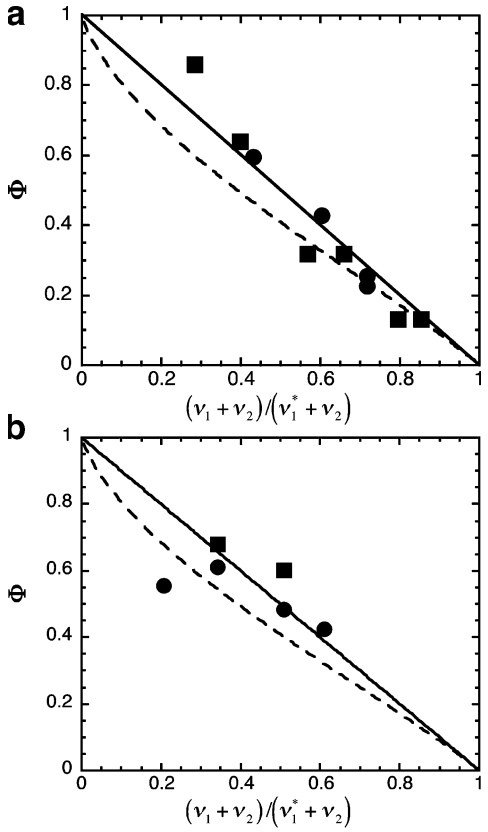

Figure 5. (a) Comparison of the stress transfer function from MD simulations of networks A obtained using a model-free approach with Flory's prediction (eq 5) for the affine model[7] (dashed curve) and Fricker prediction[8] (eq 6) for the phantom model (solid line). Note that eq 5 is valid only for complete removal of stage 1 cross-links whereas eq 6 is applicable to removal of some or all of the stage 1 cross-links. Squares represent simulations with no remaining first stage cross-links, and circles represent cases with some portion of the first stage remaining. (b) Comparison of the stress transfer function from MD simulations of networks B obtained using a model-free approach with Flory's prediction (eq 5) for the affine model[7] (dashed curve) and Fricker's prediction[8] (eq 6) for the phantom model (solid line). Here circles represent the case with initial stage 1 network chain density $\nu_1^* = 0.0041/\sigma_{LJ}^3$ and squares with $\nu_1^* = 0.0082/\sigma_{LJ}^3$. In both cases all the original stage 1 cross-links were removed.

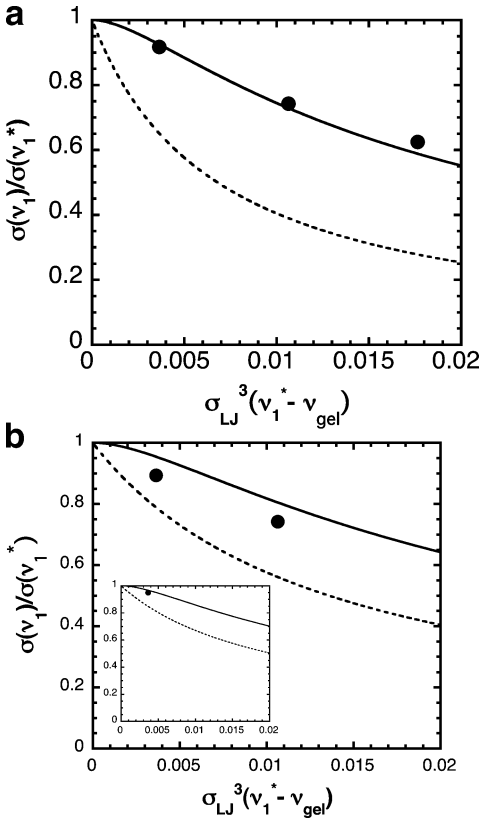

Figure 6. (a) Stress ratio for networks A, $\nu_2 = 0.0068/\sigma_{LJ}^3$, from simulation (points) compared with the phantom network prediction (dashed line) and the slip-tube mode (solid line). (b) Stress ratio for networks A, $\nu_2 = 0.0176/\sigma_{LJ}^3$, from simulation (points) compared with the phantom network prediction (dashed line) and the slip-tube mode (solid line). Inset: $\nu_2 = 0.0204/\sigma_{LJ}^3$.

$\sigma_{LJ}^3\nu_2 = 0.0068$, 0.0136, and 0.0204 and all of the stage 1 cross-links are removed. It can be seen from these figures that the affine/phantom model greatly underestimates the stress ratio since no entanglement effects are included in the theory. By contrast, the slip-tube model is in very good agreement with all the MD simulations of the A networks. Figure 7a,b shows similar comparisons with MD simulations of networks B where $\sigma_{LJ}^3(\nu_1^* - \nu_{gel}) = 0.00411$ and 0.00821. Good agreement is found between the slip-tube theory and MD simulations of both networks A and B even though the Fricker formula for Φ was derived using the phantom network model.

The data displayed in the previous figures represents cases where all of the stage 1 cross-links above gelation are removed, but it is possible to make predictions for systems with some portion of the stage 1 cross-links remaining using Fricker's formula for the effective stage 1 cross-link density, $\nu_1^{eff} = \nu_1 + \nu_2[(\nu_1^* - \nu_1)/\nu_T]$. Figure 8 shows the stress divided by the stress at a standard network chain density, $\nu_1 = 0.0176/\sigma_{LJ}^3$, for the networks A and the slip-tube model as a function of this quantity. The excellent agreement between theory and simulation suggests that the Fricker formula, obtained by considering ideal phantom networks, remains valid even for the phantom contribution in an entangled polymeric network.

The independent network hypothesis has previously been extended to any number of network formation stages for the affine[7] and the phantom models.[8,31] The stress transfer function, however, was not previously extended in the same manner. We have generated a preliminary approximate extension of the Fricker transfer function to an arbitrary number of stages, each involving scission and/or cross-linking, in a form appropriate for inclusion into finite element codes. The effective cross-link density of the *p*th stage network is, in this scheme, given by

$$\nu_p^{eff} = \nu_p\left(1 - \sum_{i=1}^{p-1}\sum_{k=p}^{n}\Phi_p^R i\right) + \sum_{i=p+1}^{n}\Phi_p^{R_i}\sum_{k=p+1}^{i}\nu_k \quad (17)$$

where

$$\Phi_p^R i = \frac{\text{cross-links created in stage } p \text{ removed in stage } i}{\text{total number of cross-links created before stage } (i+1)}$$

This extension allows the analysis of elastomers with arbitrary strain histories.

5.2. Localization of Cross-Links. In order to gain further insight into the stress transfer of stage 1 to stage 2 cross-links, we investigated whether there were differences in localization of the various types of cross-linkages. Chains are localized in space due to both entanglements and chemical cross-links in the network. This localization occurs all along the chain backbone as monomer units experience lateral fluctuations inside

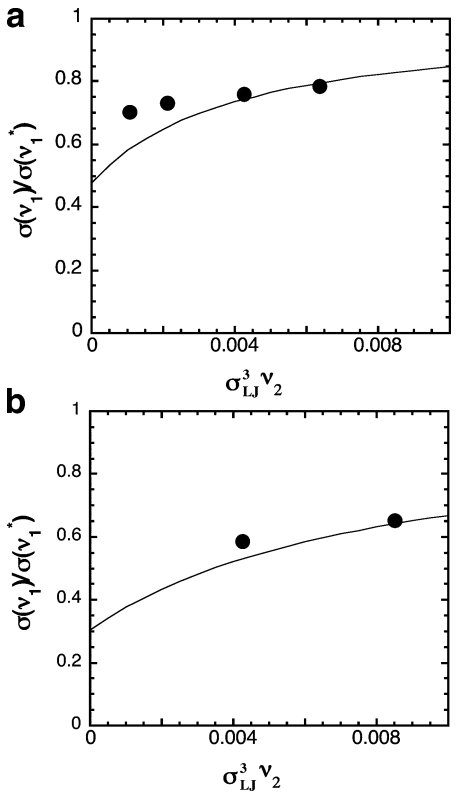

Figure 7. (a) Stress ratio for the B networks for $\nu_1^* = 0.0041/\sigma_{LJ}^3$ as a function of ν_2 when all of the original stage 1 cross-links were removed. Points are the MD simulations, and the solid curve is the prediction from the slip-tube model. (b) Stress ratio for the B networks for $\nu_1^* = 0.0086/\sigma_{LJ}^3$ as a function of ν_2 when all of the original stage 1 cross-links were removed. Points are the MD simulations, and the solid curve is the prediction from the slip-tube model.

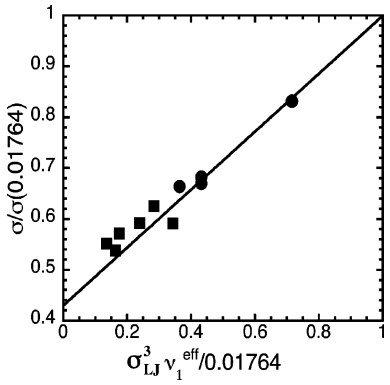

Figure 8. Relative stress (relative to stress at a standard cross-link density, $\nu_1 = 0.017644/\sigma_{LJ}^3$chosen to match the highest initial cross-link density) as a function of ν_1^{eff}. Circles represent cases where some residual first stage cross-links remain while squares represent cases with all stage 1 cross-links above gelation are removed. The line represents the slip tube prediction using Fricker's effective stress transfer function.

their entanglement tube. We have measured the mean-square displacement

$$g_\alpha(\Delta t) = \langle |r_\alpha(t + \Delta t) - r_\alpha(t)|^2 \rangle \qquad (18)$$

for the Cartesian components (denoted by α) of the cross-links averaged over all four-functional cross-links and time. At short times the mean-square displacements show subdiffusive behavior as the cross-link junctions are tethered by their pendent chains. At large times a plateau is reached. The height of this

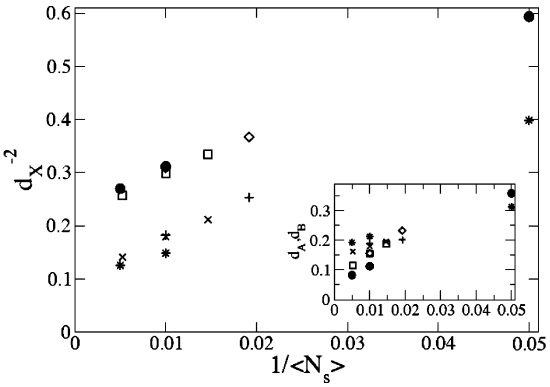

Figure 9. Localization of cross-links vs strand length for directions parallel (lower) and perpendicular (upper) to the strain direction at $\lambda_2 = 2.0$ for B networks. Stage 1 networks (circles, stars); stage 2 networks obtained from stage 1 networks with 1400 (squares, ×'s) and 2800 (diamonds, pluses) cross-links. The inset shows the cross-link d_A (circles, squares, diamonds) and entanglement d_B (stars, ×'s, pluses) to the localization.

plateau $d_{X,\alpha}^2 = g_\alpha(t \to \infty)/2$ is a direct measure of the localization experienced by the cross-links. This extrapolation is made by performing a least-square fit to the functional form

$$g(d_X^2, \zeta) = 2d_X^2[1 - \exp(-(t/\zeta d_X^4)^{1/2})]$$

to the sampled mean-square displacements.

Figure 9 shows the strength of the cross-link localization as a function of the average network chain length. Fluctuations are anisotropic and smaller in the direction perpendicular to the elongation. As the strands become longer, the network becomes softer and the fluctuations increase for both the stage 1 and 2 networks. Interestingly, the localization of the stage 2 cross-links does not seem to depend on the original cross-link density and differs slightly from the values found for pure stage 1 networks. Postcuring under strain appears to increase the localization parallel to the elongation, while fluctuations in the perpendicular direction seem only weakly affected.

The observed behavior qualitatively agrees with theoretical expectations. For stage 1 networks it was found[32] that the strain dependence of the cross-link fluctuations is well characterized by the functional form

$$d_C^{-4}(\lambda_\alpha) = d_A^{-4}(\lambda_\alpha) + \lambda_\alpha^{-2} d_B^{-4}(\lambda_\alpha) \qquad (19)$$

predicted by the double tube theory.[16] The inset of Figure 9 shows the decomposition of the cross-link localization length d_C into contributions d_A and d_B extracted from $d_X^2(\lambda_{||})$ and $d_X^2(\lambda_\perp)$. The strain-dependent contribution characterized by d_B is due to entanglements, while cross-linking chains into a network leads to a strain independent localization. In particular, one expects $d_A^2 \sim \langle N_s \rangle$ *independently of the cross-linking history*. The entanglement tube diameter should be of the order $d_B^2 \sim N_e$ independently of $\langle N_s \rangle$, where N_e denotes the entanglement length.

5.3. Microscopic Deformations. The length-scale dependent deformations of the microscopic chain conformations can be characterized by the dimensionless ratios $3\langle r_{||}^2(n,\lambda_{||})\rangle/\langle r^2(n)\rangle$ and $3\langle r_\perp^2(n,\lambda_\perp)\rangle/\langle r^2(n)\rangle$ as a function of the chemical distance n. Here the numerators are the Cartesian components of the mean-square distances parallel and perpendicular to the strain direction, while the denominator denotes the isotropic mean-square distance sampled in the unstrained state.

Figure 10 shows the microscopic deformations for stage 1 B networks compared to a corresponding stage 2 B networks in

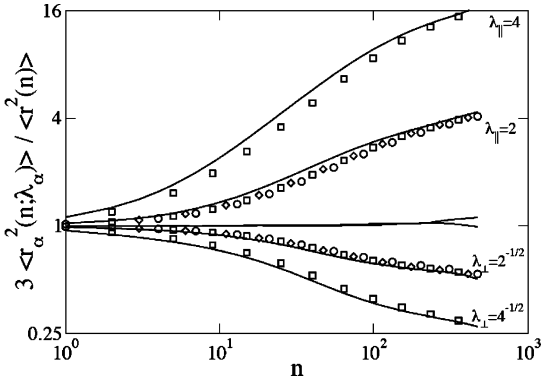

Figure 10. Scale dependence of the microscopic deformations parallel (greater than unity) and perpendicular (less than unity) to the strain direction for stage 1 and 2 B networks at strains $\lambda_2 = 1.0$, 2.0, and 4.0. Stage 1 networks with 1400 cross-links (solid lines with error bars). Stage 2 networks where the original stage 1 cross-links were removed and replaced by 700 (circles), 1400 (squares), and 2100 (diamonds) cross-links in the strained state.

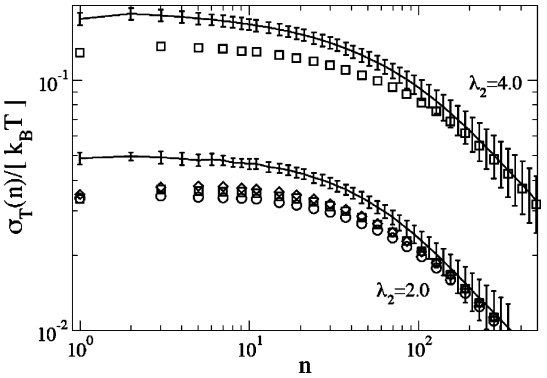

Figure 11. Scale dependence of the mesoscopic stress for stage 1 and 2 B networks at uniaxial stretch ratios of 2.0 and 4.0. Stage 1 network with 1400 cross-links (solid lines with error bars). Stage 2 networks where the original stage 1 cross-links were removed and replaced by 700 (circles), 1400 (squares), and 2100 (diamonds) cross-links in the strained state.

which various numbers of stage 1 cross-links were removed. At large chemical distances affine behavior is observed, which is expected for the deformation of a solid. At short distances, however, chain conformations are only weakly perturbed. This is a characteristic of polymeric liquids, where moderate strain causes the chemical bonds to partially align with the deformation rather than stretch. The crossover between these two regimes defines a characteristic length, which appears to be about 25% larger in stage 2 networks. This is a clear indication of partial structural relaxation of the network after the removal of the original cross-links.

The macroscopic elastic reponse of a polymer network to strain is due to the entropy loss associated with the changes of the microscopic chain conformations. Using the length-scale dependent deformations, one can define a mesoscopic stress function[13,32]

$$\sigma_T(n,\lambda) = 3k_B T \rho_s(n) \left[\frac{\langle r_{||}^2(n,\lambda_{||}) \rangle}{\langle r^2(n) \rangle} - \frac{\langle r_\perp^2(n,\lambda_\perp) \rangle}{\langle r^2(n) \rangle} \right] \quad (20)$$

from which the macroscopic stress can be estimated in the limit of $\sigma_T(n)$ as $n \to 0$. The corresponding data are shown in Figure 11. Normal stresses in stage 2 networks are nonzero but clearly lower than the corresponding stage 1 network. This is consistent with the partial transfer of stress from the stage 1 to the stage 2 cross-links. Note from Figure 11 that there is a weak but systematic dependence on the density of stage 2 networks which is barely discernible in the Figure 10 microdeformations. Such a dependence was predicted theoretically by the Flory and Fricker theories in eqs 5 and 6 for the stress transfer function Φ and is seen in Figures 1 and 5.

6. Conclusions

In this investigation we used MD simulations to investigate the effect of scission of the initial chemical network in an elastomer formed in two stages. Very good agreement with simulation was found for the stress transfer functions deduced from Gaussian and phantom theories, despite the fact that these simple theories do not include the effect of entanglements and are known to be inadequate for predicting the stress. This result suggests that these simple stress transfer functions have a broader applicability and could be applied to more rigorous models that include entanglements.

This empirical ansatz was demonstrated in this investigation by applying the stress transfer function of Fricker,[8] deduced from the phantom model, into the slip-tube model of Rubinstein and Panyukov[14] to calculate the stress from multiple stage deformations with sequential cross-linking and scission. The results reported here show that this simple approach does indeed lead to stress predictions in very good agreement with simulation. This suggests that the effect of stress transfer and multiple stage cross-linking in entangled networks could be incorporated into tube models to provide a more rigorous foundation for the treatment of chemically reacting networks.

It should be emphasized that in the investigation reported here we studied the case of sequentially removing the stage 1 cross-links with the stage 2 cross-link density held fixed. The more practical application arises when cross-linking and scission are occurring simultaneously. Although we did not consider this more general problem here, it could be also treated following the approach of Flory[7] and Fricker,[8] who did consider this case for Gaussian and phantom models.

We briefly comment on possible implications of our results for the theoretical description of stress equilibration in entangled melts of linear or branched polymers. In these systems, Brownian chain motion leads to a continuous renewal of entanglement constraints. To apply the present notation to an entangled melt after a step strain, one might distinguish between the remaining original stage 1 entanglements and the newly formed stage 2 entanglements. According to the tube model,[33] stage 2 entanglements would be found on chain portions which have left their original surroundings via reptation or contour length fluctuations. Furthermore, constraint release should lead to a gradual replacement of stage 1 entanglements along the remaining sections of the tube. Our point here is that the observation of stress transfer during the renewal process in chemically cross-linked networks sheds some doubt on the common assumption that there is no stress contribution from chain portions which have left their original tube in melts.

Acknowledgment. Sandia is a multiprogram laboratory operated by Sandia Corporation, a Lockheed Martin Company, for the United States Department of Energy's National Nuclear Security Administration under Contract DE-AC04-94AL85000. C.S. is a Steno Research Assistant Professor funded by the Danish Natural Science Research Council and gratefully acknowledges this support. The authors acknowledge Aidan Thompson whose modified LAMMPS code was used for the simulation set A presented here.

References and Notes

(1) Tobolsky, A. V. *Properties and Structure of Polymers*; Wiley: New York, 1960.
(2) Tobolsky, A. V.; Prettyman, I. B.; Dillon, J. H. *J. Appl. Phys.* **1944**, *15*, 380.
(3) Andrews, R. D.; Tobolsky, A. V.; Hanson, E. E. *J. Appl. Phys.* **1946**, *17*, 352.
(4) Curro, J. G.; Salazar, E. A. *J. Appl. Polym. Sci.* **1975**, *19*, 2571.
(5) Curro, J. G.; Salazar, E. *Rubber Chem. Technol.* **1977**, *50*, 895.
(6) Salazar, E. A.; Curro, J. G.; Gillen, K. T. *J. Appl. Polym. Sci.* **1977**, *21*, 1597.
(7) Flory, P. J. *Trans. Faraday Soc.* **1960**, *56*, 722.
(8) Fricker, H. S. *Proc. R. Soc. London A* **1973**, *335*, 269.
(9) Wineman, A. S.; Rajagopal, K. R. *Arch. Mech.* **1990**, *42*, 53.
(10) Mott, P. H.; Roland, C. M. *Macromolecules* **2000**, *33*, 4132.
(11) Santangelo, P. G.; Roland, C. M. *Rubber Chem. Technol.* **2003**, *76*, 892.
(12) Rottach, D. R.; Curro, J. G.; Grest, G. S.; Thompson, A. P. *Macromolecules* **2004**, *37*, 5468.
(13) Rottach, D. R.; Curro, J. G.; Budzien, J.; Grest, G. S.; Svaneborg, C.; Everaers, R. *Macromolecules* **2006**, *39*, 5521.
(14) Rubinstein, M.; Panyukov, S. *Macromolecules* **2002**, *35*, 6670.
(15) Everaers, R. *Eur. Phys. J. B* **1998**, *4*, 341.
(16) Mergell, B.; Everaers, R. *Macromolecules* **2001**, *34*, 5675−5686.
(17) Duering, E. R.; Kremer, K.; Grest, G. S. *Macromolecules* **1993**, *26*, 3241.
(18) Duering, E. R.; Kremer, K.; Grest, G. S. *J. Chem. Phys.* **1994**, *101*, 8169.
(19) Plimpton, S. J. *J. Comput. Phys.* **1995**, *117*, 1 (www.cs.sandia.gov/~sjplimp/lammps.html).
(20) Grest, G. S.; Kremer, K. *Macromolecules* **1990**, *23*, 4994.
(21) Grest, G. S.; Kremer, K. *J. Phys. (Paris)* **1990**, *51*, 2829.
(22) Edwards, S. F. *Proc. Phys. Soc., London* **1967**, *92*, 9.
(23) Erman, B.; Flory, P. J. *Macromolecules* **1982**, *15*, 806.
(24) Heinrich, G.; Straube, E.; Helmis, G. *Adv. Polym. Sci.* **1988**, *85*, 33.
(25) Rubinstein, M.; Panyukov, S. *Macromolecules* **1997**, *30*, 8036.
(26) Everaers, R. *New J. Phys.* **1999**, *1*, 1.
(27) Treloar, L. R. G. *The Physics of Rubber Elasticity*; Clarendon Press: Oxford, 1975.
(28) James, H. M.; Guth, E. *J. Chem. Phys.* **1943**, *11*, 455.
(29) Ronca, G.; Allegra, G. *J. Chem. Phys.* **1975**, *63*, 4990.
(30) Erman, B.; Flory, P. J. *J. Chem. Phys.* **1978**, *68*, 5363.
(31) Baxandall, L. G.; Edwards, S. F. *Macromolecules* **1988**, *21*, 1763.
(32) Svaneborg, C.; Grest, G. S.; Everaers, R. *Phys. Rev. Lett.* **2004**, *93*, 257801.
(33) McLeish, T. C. B. *Adv. Phys.* **2002**, *51*, 1379.

MA062139L